Journal of Materials Chemistry C

ROYAL SOCIETY OF CHEMISTRY

PAPER

View Article Online
View Journal | View Issue

Check for updates

Cite this: J. Mater. Chem. C, 2025, 13, 1449

Tunable color-stable hybrid white OLEDs by combining fluorescent and TADF emitters in a single emissive layer†

Upasana Deori, Thamodharan Viswanathan, Nisha Yadav and Pachaiyappan Rajamalli *

Received 13th September 2024,
Accepted 13th November 2024

DOI: 10.1039/d4tc03934c

rsc.li/materials-c

Hybrid metal-free white organic light-emitting diodes (WOLEDs) based on the complementary color of a fluorescent dopant and thermally activated delayed fluorescence (TADF) emitters in a single emissive layer structure have drawn considerable attention and achieved enormous progress for their potential in complete exciton utilisation and a simple design structure. However, WOLEDs made of a single emissive layer suffer from poor color stability and insufficient blue emission for a well-balanced white light. Here, we designed and synthesised an orange fluorescent emitter with a peak maximum at 589 nm, which was utilised in fabricating WOLEDs by combining with a robust sky-blue TADF material. The resulting hybrid WOLEDs showed remarkable electroluminescence performances with a maximum external quantum efficiency (EQE) of 23.8%, and a balanced white emission could be attained with Commission Internationale de l'Eclairage (CIE) coordinates of (0.33, 0.43). The correlated color temperature (CCT) is measured to be 5863 K, resembling the sunlight temperature at noon. Furthermore, the white light can be tuned to cool and warm white emissions by controlling the concentration of the fluorescent dopant. All the WOLEDs exhibit excellent color stability, maintaining minimal shifts in the CIE coordinates even at high brightness/voltages.

Published on 14 November 2024. Downloaded on 9/13/2025 11:55:52 PM.

1. Introduction

White organic light-emitting diodes (WOLEDs) have been considered a promising next-generation technology for flat-panel full-color displays and solid-state lighting, which opened a new market in the illumination sector due to their comprehensive merits of high efficiency, low energy consumption, low-cost, feasible flexibility, and well-balanced white color.[1–5] Extensive research on materials and device structures has been devoted to exploring WOLEDs with high emission efficiency in the past years.[6] The WOLEDs based on traditional all-fluorescent emitters can hardly exceed 25% of exciton utilisation due to theoretical limitations and end up with inadequate performance for lighting applications.[7] Alternatively, phosphorescence and thermally activated delayed fluorescence (TADF) emitters have been exploited in developing highly efficient WOLEDs due to their near unity internal quantum efficiency that can harvest all the electrically generated excitons, including the dark triplet excitons.[8–11] However, the phosphors contain expensive rare noble metals and suffer from color impurity and poor operational stability, particularly for the blue phosphorescent emitters, which remain a big obstacle and restrict their reliability in practical applications.[12–14] Conversely, all TADF WOLEDs usually suffer from serious exciton-annihilation processes, inadequate energy transfer, and dissatisfactory Commission Internationale de l'Eclairage (CIE) coordinates due to an imbalance in the radiation decay rates of the emitters, thus leading to unbalanced white emission.[15–17] To address these issues, fully organic and hybrid WOLEDs, constructed with fluorescent emitters and TADF materials, have gained noticeable attention and emerged as potential candidates to meet the aforementioned requirements.[18,19]

White devices can be achieved by combining three primary color (red, green, and blue) or two complementary color (sky blue and orange) materials in the emissive layer, thus covering the visible spectrum.[20,21] A sandwich-type emissive layer with two separate green/red layers was reported to manage excitons within their respective emissive zones, achieving a maximum external quantum efficiency (EQE) of 18.2%.[22] However, such an approach required multiple emissive layers, introducing more intricate energy transfer paths and complications in the overall fabrication process.[23–25] In principle, the WOLEDs

Materials Research Centre, Indian Institute of Science, Bangalore–560012, Karnataka, India. E-mail: rajamalli@iisc.ac.in

† Electronic supplementary information (ESI) available. CCDC 2352021. For ESI and crystallographic data in CIF or other electronic format see DOI: https://doi.org/10.1039/d4tc03934c

Published on 14 November 2024. Downloaded on 9/13/2025 11:55:52 PM.

fabricated with a single emissive layer are technically simple and potentially reduce the complexity of the device structure.[26,27] These WOLEDs can be developed by combining a blue TADF material, which also behaves as a sensitiser, with an orange fluorescent emitter. The blue TADF emitter should emit its own color as well as transfer the generated excitons from its lowest singlet level (S_1) through the forward Förster energy transfer (FRET) process to the orange fluorophore to achieve white emission. Such an energy transfer process is known as hyperfluorescence.[28–30] However, WOLEDs made of a single emissive layer suffer from low exciton utilisation, poor color stability, and lack of blue emission, resulting in unbalanced white light.[31,32] The inevitable energy loss processes, such as direct charge trapping in the fluorescent emitter and the Dexter energy transfer (DET) from the triplet state (T_1) of the TADF emitter to that of the fluorescent dopant, may contribute to the exciton loss in the device. Moreover, the sensitising FRET process often works more efficiently than the radiative decay of the blue TADF emitter, which results in inadequate blue emission.[18] This is why an extremely low doping concentration of the fluorescent dopant is adopted to minimise the energy loss mechanisms. The energy transfer process is susceptible to the concentration of the fluorescent dopant, which allows the modulation of the white light emission by varying the doping percentage in the emissive layer. For instance, Song *et al.* developed a single emissive layer WOLED with a blue TADF emitter and extremely low concentration (0.03–0.05 wt%) of the yellow fluorescent dopant and realised a maximum EQE of 15.5% and CIE of (0.28, 0.35).[33] It is challenging to control such a low concentration during fabrication. Another report by Xie *et al.* achieved an EQE of 21.8% with balanced white emission by employing a dual-host system, strategically modulating the energy transfer pathways within the emissive layer.[34] Wei *et al.* reported WOLEDs with an EQE_{max} of 19.6% and CIE coordinates of (0.33, 0.45) using sterically shielded emitters to increase the intermolecular distance and prevent exciton loss processes.[35] Numerous endeavours have been devoted to improving the performance of single emissive layer WOLEDs by choosing efficient new blue TADF emitters.[36,37] Despite these efforts, white devices still required additional enhancements in their performances, primarily due to the persisting issues of unbalanced white emission and color shifts experienced at high brightness. Moreover, tuning the emission from cool white to warm white light from the same system by adjusting the concentrations would be beneficial, and it would enable simultaneous achievement of high-efficiency and balanced white color OLEDs.

In this work, we designed and synthesised a fluorescent emitter *p*-ditolylamino anthracene carbonitrile (*p*-DTAACN), showing orange emission with a peak maximum at 589 nm and an EQE of 5.2%. Due to its broad and long-wavelength emission, the emitter is ideal for fabricating white OLEDs to cover the maximum visible spectrum. In this regard, a previously reported sky-blue TADF emitter, (3,5-bis(3,6-di-*tert*-butyl-9*H*-carbazol-9-yl)phenyl)(pyridin-3-yl)methanone, 3BPy-*m*DTC, which radiates at 479 nm with an EQE of 24.6%,[38,39] was used in constructing white light devices. By utilising these two complementary emitters, single emissive layer WOLEDs were developed. In addition, the white emission of the devices allowed the tuning of color from a cooler to a warmer tone by precisely varying the doping concentration of *p*-DTAACN from 0.5 wt% to 1.0 wt% in the emissive layer. Notably, 0.7 wt% of *p*-DTAACN exhibited a maximum EQE of 23.8% and a purer white emission with CIE coordinates of (0.33, 0.43) and a CCT of 5863 K. Furthermore, the devices also realised remarkable spectral stability in white electroluminescence (EL) spectra across varying operating voltages. These findings suggest a facile pathway for developing highly efficient and color-stable WOLEDs, offering practical applications through thoughtful design and optimisation.

2. Results and discussion

2.1. Synthesis and characterisation of the anthracene emitter

2.1.1. Molecular design and electronic structure. The design and approach of the molecular structure of the emitter were based on a push–pull strategy. It consisted of a strong donor unit, di-*p*-tolylamine (*p*TA), and a strong acceptor core, cyano (CN), which were bridged with an anthracene planar unit, as shown in Fig. 1a. The designed emitter was synthesised by a simple three-step process, and detailed synthesis procedures are given in the ESI.† The final emitter, *p*-DTAACN, was further purified by vacuum sublimation, and the chemical structure was confirmed by ^{1}H and ^{13}C NMR spectroscopic techniques and high-resolution mass spectrometry (HRMS) (Fig. S1 and S2, ESI†). *p*-DTAACN was further structurally confirmed by single-crystal X-ray diffraction studies. The single crystals of *p*-DTAACN were grown by a slow evaporation method using a DCM and methanol mixture. *p*-DTAACN was crystallised in a tetragonal crystal system, and various non-covalent interactions were observed in the crystal packing, as shown in Fig. S3 (ESI†). The thermal properties and stability of the emitter were examined through thermogravimetric analysis (TGA) and differential scanning calorimetry (DSC) under a nitrogen atmosphere. The TGA trace revealed that *p*-DTAACN exhibited high thermal stability with a decomposition temperature of 320 °C at 5% weight loss (Fig. S4a, ESI†) and the DSC plots showed a glass transition temperature (T_g) of 110 °C (Fig. S4b, ESI†).

Using the Gaussian 16 programme, density functional theory (DFT) calculations were carried out to obtain insight into the electronic states of the *p*-DTAACN molecule. The result indicates that the highest occupied molecular orbital (HOMO) is primarily distributed on the electron-donating tolylamine units and extends to the anthracene unit. The lowest unoccupied molecular orbital (LUMO) is covered by the electron-accepting cyano-anthracene group (Fig. 1b). According to these findings, *p*-DTAACN is a donor–acceptor (D–A) dipole molecule with substantial charge transfer capabilities from the donor to acceptor (HOMO to LUMO), which is consistent with the emission spectra. Furthermore, the HOMO–LUMO energy gap was found to be E_g = 1.67 eV, and the calculated singlet and

 This journal is © The Royal Society of Chemistry 2025

Published on 14 November 2024. Downloaded on 9/13/2025 11:55:52 PM.

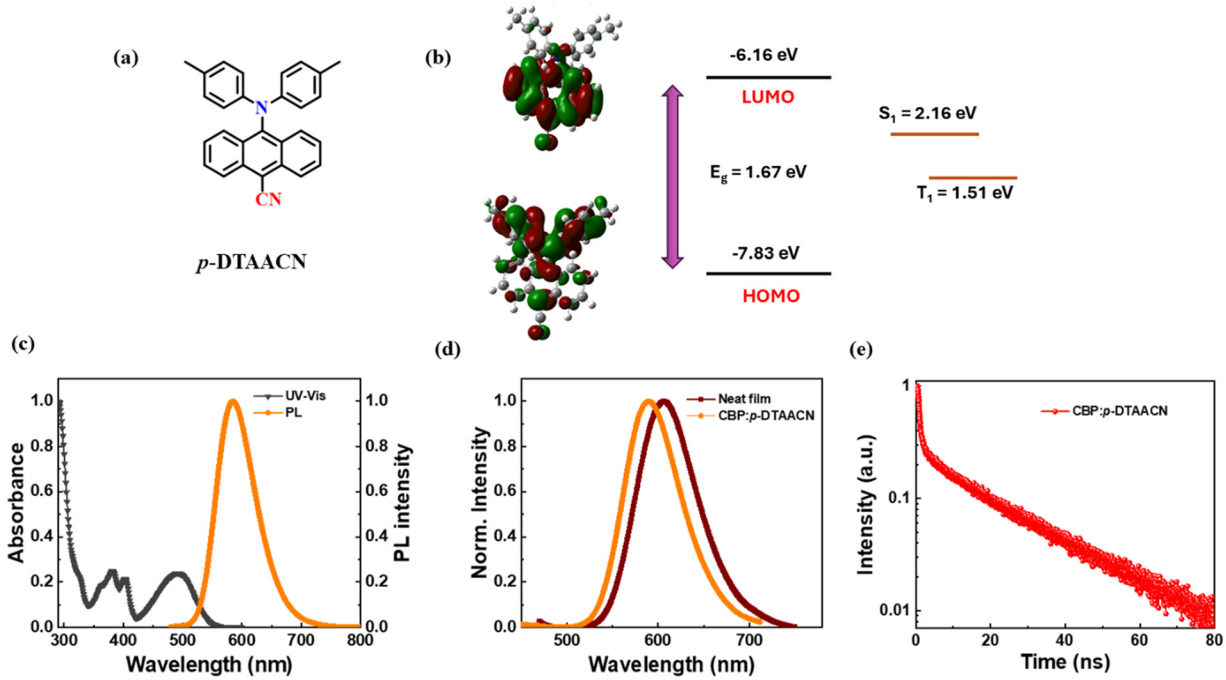

Fig. 1 (a) Molecular structure; (b) frontier orbital distribution and the calculated HOMO/LUMO energy levels and lowest singlet/triplet levels of *p*-DTAACN; (c) UV-vis absorption and fluorescence behaviour measured in 10^{-5} M toluene; (d) photoluminescence spectra of the neat film and CBP doped film of *p*-DTAACN; and (e) the transient photoluminescence decay for the CBP:*p*-DTAACN doped film with excitation wavelength 340 nm and emission wavelength 588 nm.

triplet energy levels were S_1 = 2.163 eV and T_1 = 1.510 eV. Though the emitter is a D–A compound, it is not expected to show TADF properties due to the large single-triplet gap.

2.1.2. Photophysical and electrochemical properties. The UV-visible absorption and steady-state photoluminescence (PL) measurements were recorded in 10^{-5} M toluene solution, and the spectra are shown in Fig. 1c. *p*-DTAACN showed structured absorption bands at 365 nm, 382 nm and 402 nm, corresponding to the π–π* transition of the anthracene core. The emitter also exhibited a prominent absorption band at 490 nm, attributed to the intramolecular charge transfer (ICT) transition originating from the donor to the acceptor core. The steady-state PL emission of *p*-DTAACN exhibits structureless emission with a peak maximum centred at 585 nm. A solvatochromic study was performed to investigate the ICT nature of the emitter by measuring the PL emission with varying solvent polarities. The emission spectra are broadened and red-shifted as the solvent polarity increases from hexane to DCM, thus confirming the presence of the charge transfer nature of the emitter (Fig. S5, ESI†). To further evaluate the potential of *p*-DTAACN in OLED application, PL characteristics in thin films were measured. The neat film demonstrated a PL peak at 606 nm, while the doped film of 5 wt% *p*-DTAACN in the 4,4′-bis(*N*-carbazolyl)-1,1′-biphenyl (CBP) host exhibited a blue-shifted PL peak at 588 nm (Fig. 1d) and possessed a high PL quantum yield of 75%. Next, transient PL decay was measured for the 5 wt% CBP-doped film, which showed a lifetime of 19 ns (Fig. 1e). No delayed component was observed, confirming that *p*-DTAACN is a conventional fluorescent emitter and not a TADF emitter.

The electrochemical behaviour of *p*-DTAACN was examined using the cyclic voltammetry (CV) technique to know HOMO and LUMO energy levels, and the voltammogram is shown in Fig. S6 (ESI†). The HOMO energy level for *p*-DTAACN was calculated to be −5.41 eV, obtained from the onset of oxidation potential. The corresponding LUMO energy level was estimated to be −3.03 eV from HOMO-E_g. These HOMO and LUMO values are desirable for smooth carrier injection in the device.

2.1.3. Electroluminance performance. To explore the electroluminance (EL) performance of the *p*-DTAACN emitter, the device was fabricated with the following architecture: (Fig. S7, ESI†) ITO/NPB (30 nm)/TCTA (20 nm)/CBP:5 wt% *p*-DTAACN (10 nm)/TPBi (50 nm)/Liq (2 nm)/Al (100 nm), wherein indium-tin-oxide (ITO) acts as a transparent anode, *N*,*N*′-bis(1-naphthyl)-*N*,*N*′-diphenyl-1,1′-biphenyl-4,4′-diamine (NPB) is applied as a hole injection layer, tris(4-carbazoyl-9-ylphenyl) amine (TCTA) is used as a hole transporting layer, 2,2′,2″-(1,3,5-benzinetriyl)-tris(1-phenyl)-1-*H*-benzimidazole (TPBi) is utilised as the electron transport layer, 8-hydroxyquinolinolato-lithium (Liq) is used as an electron injection layer and finally aluminum (Al) works as the cathode. The device properties shown in Fig. 2 and summarised in Table 1 display excellent electroluminance performances with a maximum luminance of 39 770 cd m^{-2} and a maximum EQE of 5.2%. The corresponding maximum current efficiency (CE) and power efficiency (PE) are 18.8 cd A^{-1} and 14.7 lm W^{-1}, respectively. The device radiated orange emission with an EL peak maximum at 589 nm, which is consistent with its PL maximum. Furthermore, the EL spectra at various operating voltages were measured (Fig. S8, ESI†), and

Published on 14 November 2024. Downloaded on 9/13/2025 11:55:52 PM.

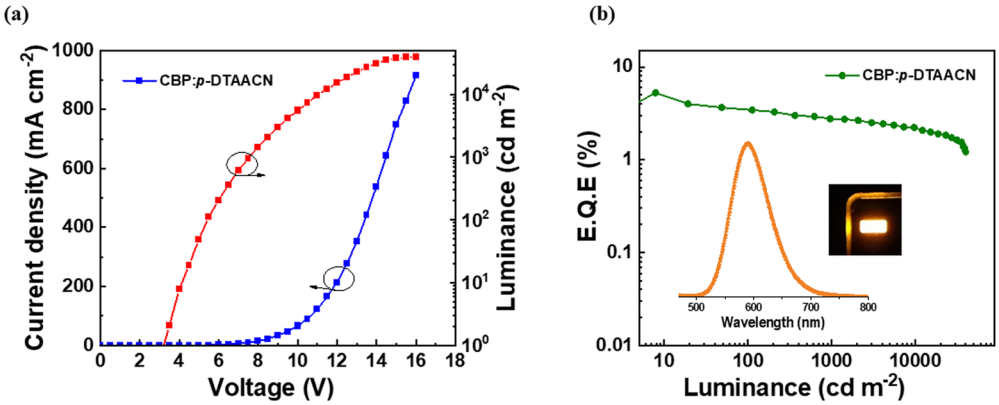

Fig. 2 (a) Dependence of current density–voltage–luminance (*J*–*V*–*L*) curve and (b) plot of external quantum efficiency *vs.* luminance of *p*-DTAACN device. Insets: Electroluminescence spectra and the photo of the *p*-DTAACN device taken at 8 V.

Table 1 Electroluminance performance of *p*-DTAACN

Device	V_{on}[a] [V]	L_{max}[b] [cd m^{-2}]	EQE[c] [%]	CE[c] [cd A^{-1}]	PE[c] [lm W^{-1}]	λ_{max}[d] [nm]	CIE[e] (x, y)
p-DTAACN	3.2	39 770	5.2	18.8	14.7	589	(0.57, 0.47)

[a] Turn-on voltage (V_{on}) at 1 cd m^{-2}. [b] Maximum luminance (L_{max}). [c] Maximum external quantum efficiency (EQE), current efficiency (CE) and power efficiency (PE) measured at the maxima. [d] Electroluminescence at peak maxima. [e] CIE coordinates recorded at 8 V.

no wavelength shift was observed, indicating the stability of EL spectra at high voltage. The CIE coordinate of the device was located at (0.57, 0.47).

2.2. Hybrid white OLEDs

Encouraged by the EL performances of *p*-DTAACN, hybrid white OLEDs were fabricated by combining this orange fluorescent emitter with a complementary robust sky-blue TADF emitter within the emissive layer. Herein, a known highly efficient sterically shielded TADF emitter, 3BPy-*m*DTC, with *tert*-butyl units, has been utilised. The peripheral inert groups present in 3BPy-*m*DTC increased the intermolecular distance between the TADF emitter and fluorescent dopant. They can strictly suppress undesired energy loss processes, such as the DET from T_1 of 3BPy-*m*DTC to T_1 of *p*-DTAACN, leading to the accumulation of triplet excitons on *p*-DTAACN and their non-radiatively decay.[38,39] In addition, 3BPy-*m*DTC has a small singlet–triplet splitting (ΔE_{ST}) of 0.05 eV, a high PLQY of 92% and an emission peak at 478 nm, and is thus preferred for effective exciton harvesting and complementary blue color. The *p*-DTAACN emitter, when precisely doped with 3BPy-*m*DTC, can span the entire visible spectrum, creating a favourable scenario for generating white light. As illustrated in Fig. 3, the TADF emitter not only emits blue light but is also employed as a sensitiser for energy transfer to the final dopant to produce orange emission, such that a well-balanced emission from both 3BPy-*m*DTC and *p*-DTAACN can be harvested for white light. As evident from Fig. S9 (ESI†), a clear overlap between the PL spectrum of 3BPy-*m*DTC and the absorption spectrum of *p*-DTAACN can be seen revealing that an efficient FRET process from S_1 of 3BPy-*m*DTC to S_1 of *p*-DTAACN is feasible. The radius

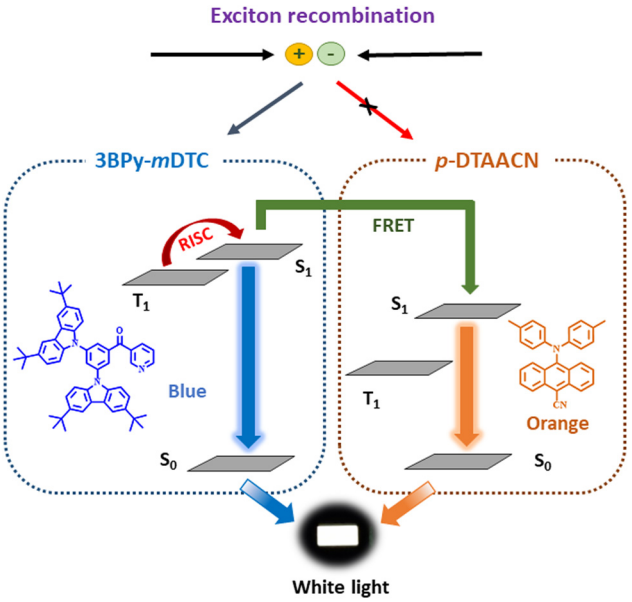

Fig. 3 A schematic representation of the energy transfer mechanism to generate white light through simultaneous emissions from both the TADF sensitiser and fluorescent emitter.

of FRET (R_0) can be expressed using the equation:

$$R_0^6 = \frac{9000\ln(10)\kappa^2\phi_f}{128\pi^5 n^4 N_A}\int_0^\infty F_D(\lambda)\varepsilon_A(\lambda)\lambda^4 d\lambda.$$

Here, $\int_0^\infty F_D(\lambda)\varepsilon_A(\lambda)\lambda^4 d\lambda$ is the spectral overlap integral between the emission spectra of the donor (3BPy-*m*DTC) and the absorption spectra of the acceptor (*p*-DTAACN).[40] κ^2 is the relative

 This journal is © The Royal Society of Chemistry 2025

Published on 14 November 2024. Downloaded on 9/13/2025 11:55:52 PM.

dipole orientation factor and taken as 2/3 for a random distribution system,[41] n is the refractive index, which is assumed to be 1.8,[42] N_A is Avogadro's number, and φ_f is the PL quantum yield of the TADF emitter in the absence of a fluorescent dopant. The R_0 value based on the spectral overlap for 3BPy-*m*DTC:*p*-DTAACN was estimated to be 5.78 nm, thus validating the effectiveness of the FRET process.

2.2.1. Device performance of white OLEDs. The two-emitter single emissive layer white OLED was designed and fabricated with the following configuration: ITO/NPB (30 nm)/TAPC (20 nm)/*m*CBP:7 wt% 3BPy-*m*DTC:0.7 wt% *p*-DTAACN (10 nm)/PPT (10 nm) TPBi (50 nm)/Liq (2 nm)/Al (100 nm), (W1). Here, to accommodate the blue TADF emitter in the emissive layer, a wide triplet energy gap host 3,3′-bis(*N*-carbazolyl)-1,1′-biphenyl (*m*CBP) was selected. 1,1-Bis[4-[*N*,*N*′-di(*p*-tolyl)amino]phenyl]cyclo-hexane (TAPC) was adopted as the hole transport layer and 2,8-bis(diphenyl-phosphoryl)-dibenzo[*b*,*d*]thiophene (PPT) served as the exciton blocking layer. PPT has deep HOMO energy levels and poor hole mobility, which can prevent holes from recombining in the interface and reduce exciton loss. The white device was developed by incorporating *m*CBP, 3BPy-*m*DTC and *p*-DTAACN within the same layer. The energy level diagram is shown in Fig. 4a, where the HOMO and LUMO levels of all layers are aligned with minimum barrier, indicating the smooth injection of holes and electrons into the emissive layer. After exciton formation, 3BPy-*m*DTC emits as well as transfers the energy to *p*-DTAACN for both simultaneous blue and orange radiation. The large spectral overlap between the absorption of *p*-DTAACN and emission of 3BPy-*m*DTC enhances the effectiveness of the FRET process, which can limit blue light emission in the white OLEDs. Therefore, a low doping concentration of *p*-DTAACN is essential in the emissive layer for pure white color and efficient performances. A slight increase in the concentration of *p*-DTAACN can facilitate the transfer of all the excitons and end up with only orange emission. In addition, such a low concentration also helps mitigate direct charge trapping on *p*-DTAACN, leading to the exciton loss process and poor device performance. Hence, the doping percentage of *p*-DTAACN in the emissive layer plays a crucial role in managing the energy transfer process.

The *J*–*V*–*L* characteristics of W1 plotted in Fig. S10a (ESI†) suggest good electrical conductivity with a turn-on voltage of 3.6 V. The WOLED showcased high efficiency as described by the EQE-Luminance characteristics in Fig. 4b, with a maximum EQE, PE and CE of 23.8%, 57.9 lm W^{-1} and 73.7 cd A^{-1}, respectively. The luminance value of W1 reached a maximum of 29 003 cd m^{-2}. The steric protection in 3BPy-*m*DTC inhibited the DET and blocked exciton loss in the device, thus being responsible for higher efficiency.[43,44] The EL spectra of W1 are shown in Fig. 4c, where two main emission bands are clearly visible with peak maxima at 476 and 560 nm, corresponding to the contribution of 3BPy-*m*DTC and *p*-DTAACN, respectively. The emission intensities of both blue and orange peaks are identical, thus displaying a pure white color. The CIE coordinates of W1 are (0.33, 0.43), and the correlated color temperature (CCT) is measured to be 5863 K, closely resembling the temperature of daylight at noon.[45,46]

To further understand the impact of varying *p*-DTAACN doping concentration on the emission pattern and color of

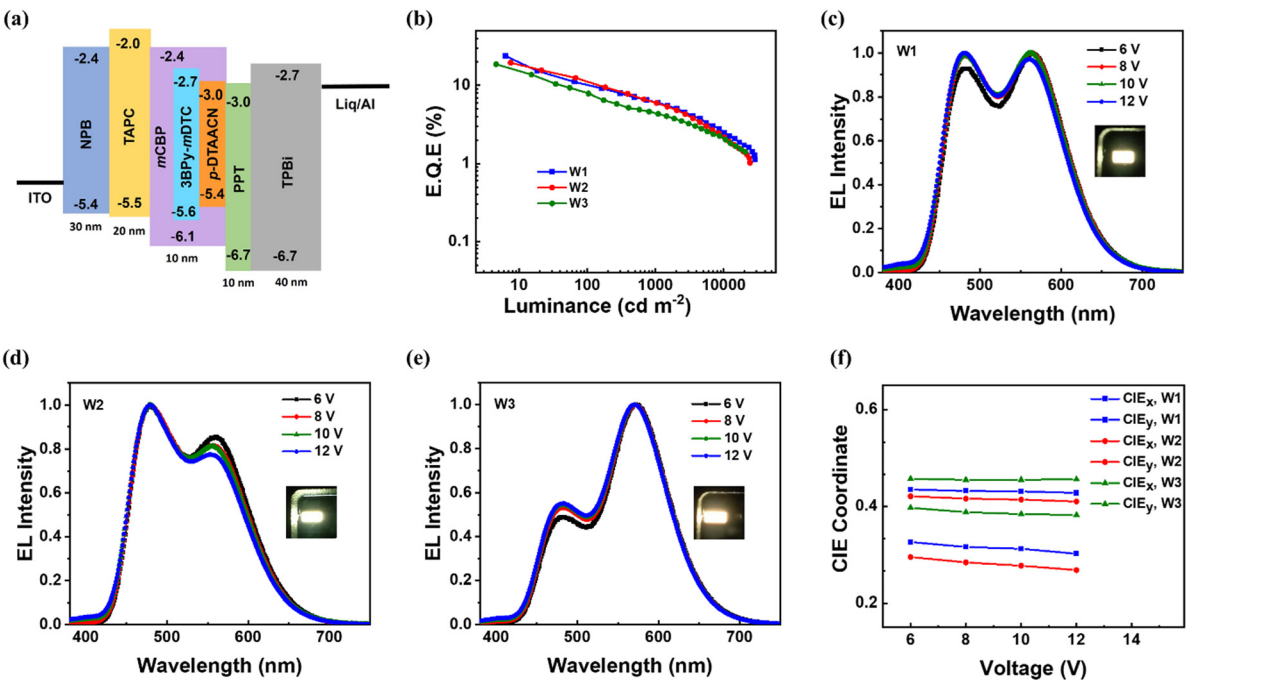

Fig. 4 (a) The energy level diagram of the hybrid white organic light-emitting diode (WOLED) structure; (b) EQE–luminescence plots of the white devices W1, W2 and W3; (c)–(e) EL spectra of W1–W3 at different voltages and the inset shows the photographs of the respective WOLEDs; and (f) CIE coordinate behaviour at various operating voltages.

Published on 14 November 2024. Downloaded on 9/13/2025 11:55:52 PM.

Table 2 Summary of the electroluminescence performance of the fabricated single emissive layer WOLEDs, W1–W3

Device	V_{on}[a] [V]	L_{max}[b] [cd m^{-2}]	EQE[c] [%]	CE[c] [cd A^{-1}]	PE[c] [lm W^{-1}]	CIE[d] (x, y)	CCT[d] [K]
W1	3.6	29 003	23.8	73.7	57.9	(0.33, 0.43)	5863
W2	3.6	24 239	19.6	60.2	42.1	(0.29, 0.42)	6863
W3	3.5	20 763	18.7	57.4	39.7	(0.39, 0.46)	4350

[a] Turn-on voltage (V_{on}) at 1 cd m^{-2}. [b] Maximum luminance (L_{max}). [c] Maximum external quantum efficiency (EQE), current efficiency (CE) and power efficiency (PE) measured at the maxima. [d] CIE coordinates and CCT recorded at 8 V.

white light, two devices (W2 and W3) were constructed with increasing and decreasing percentage of *p*-DTAACN doping compared to W1. The device structure mirrored that of W1, except for the emissive layer, where W2 contained 0.5 wt% *p*-DTAACN while W3 contained 1.0 wt%. Fig. 4 compares the electroluminescence performances of the WOLEDs, and the detailed parameters are illustrated in Table 2. W2 and W3 both displayed commendable performances, and their maximum EQE values were 19.6% and 18.7%, respectively. The maximum PE and CE values for W2 and W3 are 42.1 lm W^{-1}, 53.7 lm W^{-1} and 60.2 cd A^{-1}, 68.4 cd A^{-1}, respectively (Fig. S10b, ESI†). The performances of W2 and W3 are slightly inferior to W1; however, the color tunability of the WOLEDs could be achieved. The EL spectra of W2 and W3 are shown in Fig. 4(d and e), along with their photographs. W2 depicted a cooler tone of white light attributed to an intensified blue region with a CIE of (0.29, 0.42) and a CCT of 6863 K measured at 8 V, implying that the majority of excitons in the emissive layer are consumed for blue emission rather than being transferred to *p*-DTAACN. As the concentration of *p*-DTAACN increased to 1.0 wt%, the CIE coordinates and CCT of W3 gradually moved from a cooler to a warmer region of (0.39, 0.46) and 4350 K, respectively. The standard reference considered for illumination applications is mostly warm white light known for its human-eye-friendly characteristics and has a CIE of (0.44, 0.40), representing a dominant orange region.[47,48] Device W3 displayed such eye-protecting warm color, close to the standard warm light, with reasonably low blue intensity and enhanced orange emission. It is noteworthy that with varying concentrations of *p*-DTAACN from 0.5 wt% to 1.0 wt%, the WOLEDs could tune the light with cool, pure and warm white emissions. The color rendering index (CRI) was also measured for the WOLEDs,[49,50] with values of 62 for W1 and 60 for both W2 and W3.

Additionally, the devices exhibited color-stable white EL spectra at various driving voltages. The CIE–voltage curve (Fig. 4f) vividly demonstrated higher spectral stability of devices W1–W3. As the voltage increases from 6 V to 12 V, a minimal spectral change in the EL spectra and a slight deviation in the CIE coordinates were observed. The luminance at 6 and 12 V ranges from ~300 to 10 000 cd m^{-2}, revealing the uniform exciton recombination zones for devices W1–W3 across a broad luminance range.

2.2.2. Investigation of the energy transfer process. The blending of complementary color emitters in the emissive layer seems to be a straightforward method to fabricate WOLEDs. However, this structural approach often encounters poor color stability and utilises conventional dopants with fast singlet radiative decay rates (k_r^s), thereby radiating insufficient blue light and leading to imbalanced white emission. Interestingly, our developed WOLEDs (W1–W3) demonstrated efficient EL performances while maintaining stable white light even at 12 V. To understand the influence of the energy transfer processes within the emissive system, the transient PL decay behaviours of the *m*CBP blended films were investigated. For comparison, the prompt and delayed lifetimes of the *m*CBP:7 wt% 3BPy-*m*DTC film without a dopant were recorded and measured to be 7.4 ns and 48.4 μs, respectively (Fig. S11, ESI†), with k_r^s of 8.9 × 10^7 s^{-1}.[51] Meanwhile, the *p*-DTAACN doped film possessed k_r^s of 3.9 × 10^7 s^{-1}, which is lower than that of the TADF emitter, 3BPy-*m*DTC. The relatively slow decay rate of *p*-DTAACN proved advantageous in competing against the fast 3BPy-*m*DTC emission, resulting in satisfactory blue and orange radiation.

Next, the transient PL decay curves of the doped white films, *m*CBP:7 wt% 3BPy-*m*DTC:*x* wt% *p*-DTAACN where x = 0.5, 0.7 and 1.0 for film 1, film 2 and film 3, respectively, were recorded at emission peak maxima at 476 nm and 560 nm. The decay curves are shown in Fig. 5 and Fig. S12 (ESI†). It is noted that film 1 exhibited a reduced delayed lifetime of 32.1 μs at 476 nm, compared to the 3BPy-*m*DTC film without a dopant (48.4 μs), suggesting that the energy transfer process occurred effectively from the 3BPy-*m*DTC to the *p*-DTAACN dopant. The delayed lifetime at 560 nm was 22.7 μs, longer than that for the *p*-DTAACN film, indicating the contribution of triplet excitons in the emission. For film 2, the delayed lifetime is 22.5 μs,

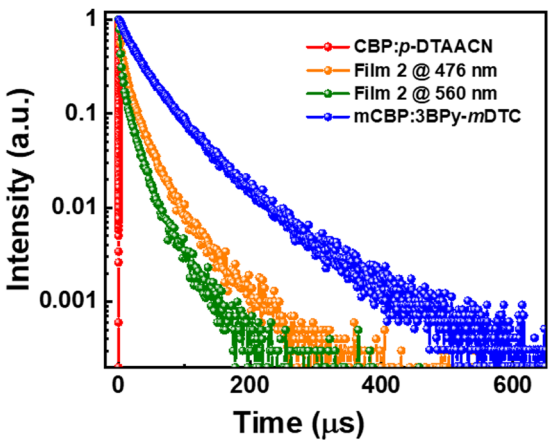

Fig. 5 Transient photoluminescence decay curves of doped white film 2, observed at the PL emission peaks at 476 nm and 560 nm, overlay with CBP:*p*-DTAACN (emission wavelength 588 nm) and mCBP:7 wt% 3BPy-mDTC (emission wavelength 479 nm) films. The excitation wavelength of 340 nm was used for all the films.

 This journal is © The Royal Society of Chemistry 2025

Published on 14 November 2024. Downloaded on 9/13/2025 11:55:52 PM.

shorter than that for film 1, which is due to the increased concentration of *p*-DTAACN, thus enhancing the FRET process. As previously stated, k_r^s of 3BPy-*m*DTC is faster than that of *p*-DTAACN; hence, excitons of 3BPy-*m*DTC can radiate quickly and with efficient FRET, the transferred excitons can also decay rapidly. The W1 device, in particular, observed a purer white colour attributed to the balanced k_r^s between the blue emission of 3BPy-*m*DTC and the orange emission of *p*-DTAACN, which could be the reason for achieving a well-balanced white light within the system and showcasing high electroluminescence performance. On further increasing *p*-DTAACN doping percentage, film 3 exhibited even shorter delayed lifetimes of 19.9 μs in comparison to film 1 and film 2. The increased concentration of *p*-DTAACN in the film induced a strong energy transfer process from 3BPy-*m*DTC to *p*-DTAACN, leading to a dramatic decrease in the delayed lifetime. Consequently, the performances demonstrated that both blue and orange components are highly sensitive over *p*-DTAACN doping concentration in the emitting layer, and with precise control, the devices hold potential in tuning the color from cool white to warm white emission. Also, by selecting appropriate sky-blue and orange emitters with balanced radiative decay rates, simultaneous realisation of high efficiency and color-stable white light is possible in single emissive layer WOLEDs.

3. Conclusions

In summary, an orange emitter, *p*-DTAACN, based on the anthracene core was synthesised which showed a maximum EQE of 5.2% and an EL peak at 589 nm. By combining this material with the sky-blue TADF emitter 3BPy-*m*DTC, efficient, spectral stable and color-tunable single emissive layer WOLEDs were successfully fabricated. The steric protection in the blue emitter helped in blocking the energy loss processes and provided maximum exciton utilisation. The white devices can be tuned from cool, pure and warm white emission with control over the *p*-DTAACN doping concentration in the range of 0.5–1.0 wt%, thereby modulating the energy transfer process. The well-balanced white device achieved an EQE_{max} of 23.8%, a PE_{max} of 57.9 lm W^{-1}, CIE coordinates of (0.33, 0.43), and a CCT of 5863 K, respectively. The radiative decay rates of both blue and orange emitters complement each other, and with the optimised concentration of *p*-DTAACN, sufficient blue light can be produced, which benefits in balancing the white emission. The results presented can bring new insights and testify the potential of WOLEDs in designing highly efficient, color-stable and human-eye-friendly light sources that may broaden our scope of mind for future lighting applications.

Data availability

Data of this paper is available from authors based on request.

Conflicts of interest

The authors declare no conflict of interest.

Acknowledgements

The authors are extremely grateful to the Department of Science and Technology (DSTFIST: SR/FST/PSII009/2010) for the instrumental facility at MRC, IISc, and SAMat Research Facilities, JNCASR, Bengaluru, for lifetime measurement facilities. The authors thank the Indian Science Technology and Engineering Facilities Map (I-STEM) for enabling access to the SC-XRD, Bruker LT D8 Quest at Indian Institute of Science, Bangalore, to carry out this work. P. R. thanks IISc and the Science & Engineering Research Board (SERB), India, for the SERB-Power Grant (SPG) (Grant no. SPG/2020/000107). T. V. thanks Science and Engineering Research Board (SERB), India, for a National Postdoctoral fellowship (NPDF-File no. PDF/2023/001648).

References

1 J. Kido, K. Hongawa, K. Okuyama and K. Nagai, *Appl. Phys. Lett.*, 1994, **64**, 815–817.
2 J. Kido, M. Kimura and K. Nagai, *Science*, 1995, **267**, 1332–1334.
3 S. Reineke, F. Lindner, G. Schwartz, N. Seidler, K. Walzer, B. Lüssem and K. Leo, *Nature*, 2009, **459**, 234–238.
4 M. Du, Y. Feng, D. Zhu, T. Peng, Y. Liu, Y. Wang and M. R. Bryce, *Adv. Mater.*, 2016, **28**, 5963–5968.
5 Z. Wu, Y. Liu, L. Yu, C. Zhao, D. Yang, X. Qiao, J. Chen, C. Yang, H. Kleemann, K. Leo and D. Ma, *Nat. Commun.*, 2019, **10**, 2380.
6 X. Tang, X.-Y. Liu, Z.-Q. Jiang and L.-S. Liao, *Adv. Funct. Mater.*, 2019, **29**, 1807541.
7 M. Strukelj, R. H. Jordan and A. Dodabalapur, *J. Am. Chem. Soc.*, 1996, **118**, 1213–1214.
8 S. Lee, H. Shin and J.-J. Kim, *Adv. Mater.*, 2014, **26**, 5864–5868.
9 D. Zhang, M. Cai, Y. Zhang, D. Zhang and L. Duan, *ACS Appl. Mater. Interfaces*, 2015, **7**, 28693–28700.
10 J. Liang, C. Li, X. Zhuang, K. Ye, Y. Liu and Y. Wang, *Adv. Funct. Mater.*, 2018, **28**, 1707002.
11 D. de, S. Pereira, P. L. dos Santos, J. S. Ward, P. Data, M. Okazaki, Y. Takeda, S. Minakata, M. R. Bryce and A. P. Monkman, *Sci. Rep.*, 2017, **7**, 6234.
12 Q. Wang and D. Ma, *Chem. Soc. Rev.*, 2010, **39**, 2387–2398.
13 Y. Zhang, J. Lee and S. R. Forrest, *Nat. Commun.*, 2014, **5**, 5008.
14 P. Heimel, A. Mondal, F. May, W. Kowalsky, C. Lennartz, D. Andrienko and R. Lovrincic, *Nat. Commun.*, 2018, **9**, 4990.
15 D. Luo, Q. Chen, Y. Gao, M. Zhang and B. Liu, *ACS Energy Lett.*, 2018, **3**, 1531–1538.
16 J. Zhao, X. Chen, Z. Yang, Z. Chi, Z. Yang, Y. Zhang, J. Xu, Z. Chi and M. P. Aldred, *J. Mater. Chem. C*, 2018, **6**, 3226–3232.

Published on 14 November 2024. Downloaded on 9/13/2025 11:55:52 PM.

17 D. Zhang, X. Cao, Q. Wu, M. Zhang, N. Sun, X. Zhang and Y. Tao, *J. Mater. Chem. C*, 2018, **6**, 3675–3682.
18 T. Higuchi, H. Nakanotani and C. Adachi, *Adv. Mater.*, 2015, **27**, 2019–2023.
19 Z. Wang, X.-L. Li, Z. Ma, X. Cai, C. Cai and S.-J. Su, *Adv. Funct. Mater.*, 2018, **28**, 1706922.
20 Z. Wu, L. Yu, X. Zhou, Q. Guo, J. Luo, X. Qiao, D. Yang, J. Chen, C. Yang and D. Ma, *Adv. Opt. Mater.*, 2016, **4**, 1067–1074.
21 T. Higuchi, H. Nakanotani and C. Adachi, *Adv. Mater.*, 2015, **27**, 2019–2023.
22 Z. Wu, Q. Wang, L. Yu, J. Chen, X. Qiao, T. Ahamad, S. M. Alshehri, C. Yang and D. Ma, *ACS Appl. Mater. Interfaces*, 2016, **8**, 28780–28788.
23 H. Liu, J. Chen, Y. Fu, Z. Zhao and B. Z. Tang, *Adv. Funct. Mater.*, 2021, **31**, 2103273.
24 Y. Chen, Q. Sun, Y. Dai, D. Yang, X. Qiao and D. Ma, *J. Mater. Chem. C*, 2020, **8**, 13777–13785.
25 X. Tang, Y. Li, Y.-K. Qu, C.-C. Peng, A. Khan, Z.-Q. Jiang and L.-S. Liao, *Adv. Funct. Mater.*, 2020, **30**, 1910633.
26 W. Song, I. Lee and J. Y. Lee, *Adv. Mater.*, 2015, **27**, 4358–4363.
27 J. Zhang, C. Han, F. Du, C. Duan, Y. Wei and H. Xu, *Adv. Funct. Mater.*, 2020, **30**, 2005165.
28 H. Nakanotani, T. Higuchi, T. Furukawa, K. Masui, K. Morimoto, M. Numata, H. Tanaka, Y. Sagara, T. Yasuda and C. Adachi, *Nat. Commun.*, 2014, **5**, 4016.
29 U. Deori, N. Yadav, G. P. Nanda, K. L. Kumawat and P. Rajamalli, *ACS Appl. Electron. Mater.*, 2023, **5**, 4959–4967.
30 U. Deori, G. P. Nanda, C. Murawski and P. Rajamalli, *Chem. Sci.*, 2024, **15**, 17739–17759.
31 B. Zhao, T. Zhang, W. Li, Z. Su, B. Chu, X. Yan, F. Jin, Y. Gao and H. Wu, *Org. Electron.*, 2015, **23**, 208–212.
32 Y.-N. Hu, X.-C. Fan, F. Huang, Y.-Z. Shi, H. Wang, Y.-C. Cheng, M.-Y. Chen, K. Wang, J. Yu and X.-H. Zhang, *Adv. Opt. Mater.*, 2023, **11**, 2202267.
33 W. Song, I. H. Lee, S.-H. Hwang and J. Y. Lee, *Org. Electron.*, 2015, **23**, 138–143.
34 F. M. Xie, S. J. Zou, Y. Li, L. Y. Lu, R. Yang, X. Y. Zeng, G. H. Zhang, J. Chen and J. X. Tang, *ACS Appl. Mater. Interfaces*, 2020, **12**, 16736–16742.
35 P. Wei, D. Zhang and L. Duan, *Adv. Funct. Mater.*, 2020, **30**, 1–10.
36 S.-J. Zou, F.-M. Xie, Y.-Q. Li, Y.-Z. Shi, Y. Shen, Z.-G. Ma, J.-D. Chen, H.-X. Wei, X.-H. Zhang and J.-X. Tang, *Mater. Today Energy*, 2021, **21**, 100745.
37 Z. Liu, B. Zhao, Y. Gao, H. Chen, B. Dong, Y. Xu, J. Li, H. Wang and W. Li, *Opt. Mater.*, 2020, **110**, 110510.
38 P. Rajamalli, V. Thangaraji, N. Senthilkumar, C. C. Ren-Wu, H. W. Lin and C. H. Cheng, *J. Mater. Chem. C*, 2017, **5**, 2919–2926.
39 B. Sk, E. Ravindran, U. Deori, N. Yadav, G. P. Nanda and P. Rajamalli, *J. Mater. Chem. C*, 2022, **10**, 4886–4893.
40 K. Gao, K. Liu, X. L. Li, X. Cai, D. Chen, Z. Xu, Z. He, B. Li, Z. Qiao, D. Chen, Y. Cao and S. J. Su, *J. Mater. Chem. C*, 2017, **5**, 10406–10416.
41 H. Wang, B. Yue, Z. Xie, B. Gao, Y. Xu, L. Liu, H. Sun and Y. Ma, *Phys. Chem. Chem. Phys.*, 2013, **15**, 3527.
42 N. Aizawa, S. Shikita and T. Yasuda, *Chem. Mater.*, 2017, **29**, 7014–7022.
43 D. Zhang, X. Song, M. Cai and L. Duan, *Adv. Mater.*, 2018, **30**, 1705250.
44 W. Xie, X. Peng, M. Li, W. Qiu, W. Li, Q. Gu, Y. Jiao, Z. Chen, Y. Gan, K. K. Liu and S.-J. Su, *Adv. Opt. Mater.*, 2022, **10**, 2200665.
45 J.-H. Jou, M.-H. Wu, S.-M. Shen, H.-C. Wang, S.-Z. Chen, S.-H. Chen, C.-R. Lin and Y.-L. Hsieh, *Appl. Phys. Lett.*, 2009, **95**, 13307.
46 J. Zhou, Z. Kou, L. Wang, B. Wang, X. Chen, X. Sun and Z. Zheng, *J. Phys. D: Appl. Phys.*, 2021, **54**, 265107.
47 G. Schwartz, S. Reineke, T. C. Rosenow, K. Walzer and K. Leo, *Adv. Funct. Mater.*, 2009, **19**, 1319–1333.
48 J. Jou, C. Hsieh, J. Tseng, S. Peng, Y. Jou, J. H. Hong, S. Shen, M. Tang, P. Chen and C. Lin, *Adv. Funct. Mater.*, 2013, **23**, 2750–2757.
49 Y. Miao, G. Wang, M. Yin, Y. Guo, B. Zhao and H. Wang, *Chem. Eng. J.*, 2023, **461**, 141921.
50 L. Lu, Y. Guo, B. Zhao, H. Wang and Y. Miao, *Mater. Today*, 2024, **74**, 109–120.
51 N. Yadav, U. Deori, E. Ravindran, B. Sk and P. Rajamalli, *J. Mater. Chem. C*, 2023, **11**, 16368–16376.

 This journal is © The Royal Society of Chemistry 2025